Nuclear Medicine and Biology 116–117 (2023) 108312

Contents lists available at ScienceDirect

Nuclear Medicine and Biology

journal homepage: www.elsevier.com/locate/nucmedbio

A radioiodinated rucaparib analogue as an Auger electron emitter for cancer therapy

Gianluca Destro [a,b,1], Zijun Chen [b], Chung Ying Chan [a], Claudia Fraser [a], Gemma Dias [a], Michael Mosley [a], Florian Guibbal [a], Veronique Gouverneur [b], Bart Cornelissen [a,c,*]

[a] Oxford Institute for Radiation Oncology, Department of Oncology, University of Oxford, Old Road Campus Research Building, Off Roosevelt Drive, OX3 7DQ Oxford, UK

[b] Department of Chemistry, Chemistry Research Laboratory, University of Oxford, 12 Mansfield Road, Oxford, OX1 3TA, UK

[c] Department of Nuclear Medicine and Molecular Imaging, University Medical Center Groningen, University of Groningen, Groningen, the Netherlands

ARTICLE INFO

Keywords:
Targeted radionuclide therapy
Auger emitter
Pancreatic cancer
SPECT imaging
Radiochemistry

ABSTRACT

Introduction: Radioligand therapy (RLT) is an expanding field that has shown great potential in the fight against cancer. Radionuclides that can be carried by selective ligands such as antibodies, peptides, and small molecules targeting cancerous cells have demonstrated a clear improvement in the move towards precision medicine. Poly (ADP-ribose) polymerase (PARP) is a family of enzymes involved in DNA damage repair signalling pathway, with PARP inhibitors olaparib, talazoparib, niraparib, veliparib, and rucaparib having FDA approval for cancer therapy in routine clinical use. Based on our previous work with the radiolabelled PARP inhibitor [^{18}F]rucaparib, we replaced the fluorine-18 moiety, used for PET imaging, with iodine-123, a radionuclide used for SPECT imaging and Auger electron therapy, resulting in 8-[^{123}I]iodo-5-(4-((methylamino)methyl)phenyl)-2,3,4,6-tetrahydro-1H-azepino[5,4,3-*cd*]indol-1-one, ([^{123}I]**GD1**), as a potential radiopharmaceutical for RLT.
Methods: [^{123}I]**GD1** was synthesized *via* copper-mediated radioiodination from a selected boronic esters precursor. *In vitro* uptake, retention, blocking, and effects on clonogenic survival with [^{123}I]**GD1** treatment were tested in a panel of cancer cell lines. Enzymatic inhibition of PARP by **GD1** was also tested in a cell-free system. The biodistribution of [^{123}I]**GD1** was investigated by SPECT/CT in mice following intravenous administration.
Results: Cell-free enzymatic inhibition and *in vitro* blocking experiments confirmed a modest ability of **GD1** to inhibit PARP-1, IC_{50} = 239 nM. *In vitro* uptake of [^{123}I]**GD1** in different cell lines was dose dependent, and radiolabelled compound was retained in cells for >2 h. Significantly reduced clonogenic survival was observed *in vitro* after exposure of cells for 1 h with as low as 50 kBq of [^{123}I]**GD1**. The biodistribution of [^{123}I]**GD1** was further characterized *in vivo* showing both renal and hepatobiliary clearance pathways with a biphasic blood clearance.
Conclusion: We present the development of a new theragnostic agent based on the rucaparib scaffold and its evaluation in *in vitro* and *in vivo* models. The data reported show that [^{123}I]**GD1** may have potential to be used as a theragnostic agent.

1. Introduction

Solid tumors are generally treated with a combination of surgery, chemotherapy, and radiotherapy. External beam radiotherapy (EBRT), which induces DNA damage and can lead to apoptosis and tumour regression, is used in approximately 50 % of cancer patients [1,2]. However, EBRT is not effective for treating metastatic or occult out-of-field disease [3,4]. Over the past decades, radioligand therapy (RLT) has emerged as a promising tool in the fight against cancer [5]. RLT is markedly distinct from classical EBRT: a radiolabelled compound is administered parenterally or orally and localizes to tumorous tissue where it emits ionizing radiation in the form of alpha, beta or Auger electron (AE) particles [6]. This causes DNA damage, tumour cell death, and tumour regression. ^{123}I emits short-range Auger electrons that

* Corresponding author at: University Medical Center Groningen, University of Oxford, CRUK/MRC Oxford Institute for Radiation Oncology, Department of Oncology, Old Road Campus Research Building, Off Roosevelt Drive, Oxford OX3 7DQ, UK.
E-mail addresses: gianluca.destro@unito.it (G. Destro), b.t.cornelissen@umcg.nl (B. Cornelissen).
[1] Present address.

https://doi.org/10.1016/j.nucmedbio.2022.108312
Received 21 November 2022; Received in revised form 21 December 2022; Accepted 22 December 2022
Available online 28 December 2022

deposit their energy over nanometre distances, resulting in high liner energy transfer (LET) [7]. Therefore, it is crucial that the radioactive drug localizes close to its most effective target, the DNA within the tumour cell nucleus. This also avoids potential crossfire effects to surrounding healthy cells [8]. To achieve selective delivery of AE-emitting radionuclides to tumors for cancer treatment, the radionuclide is attached to a targeting ligand [9]. Thanks to PARP-1 nuclear localization selective PARP inhibitors seem excellent candidates as vehicles for Auger-electron emitting radionuclides [10].

PARP enzymes (PARP-1, PARP-2, and PARP-3) play a central role in DNA damage repair signalling pathway and become active by binding to damaged DNA [11]. When a PARP inhibitor binds to the PARP enzyme, it can trap the enzyme to the damaged DNA impairing the process of single-strand break repair by inhibiting the catalytic activity of the DNA damage repair enzyme. Therefore, the complex formed by the trapped DNA and PARP enzyme causes the stalling and collapse of replication forks leading to double-strand break formation. These damages require homologous recombination (HR) for being repaired, therefore, cancer cells with anomalies in HR genes, such as *BRCA1/2*, cannot repair DSBs, causing cell death [12]. Thanks to this DNA trapping, in addition to the increased expression of PARP protein in tumour tissue *versus* surrounding normal tissue and the short range of AEs, AE-radiolabelled compounds targeting PARP represent an excellent vehicle for radioligand therapy [13]. Several research groups, including Reiner [14–16], Mach [17–19] and Morgenroth [20], have already developed radiolabelled PARP-binding compounds for RLT based on a variety of PARP inhibitor scaffolds, mainly built on olaparib and rucaparib variants (Fig. 1). Our group recently reported the radiosynthesis of [^{18}F]olaparib [21], [^{18}F]AZD2461 [22] and [^{18}F]rucaparib [23,24], demonstrating the strength of copper mediated radiofluorination as a useful methodology to overcome the challenge of C—^{18}F bond formation [25,26] and that radiolabelled versions of PARP inhibitors can prove to be useful PET imaging agents [27,28]. Radioiodinated versions of PARP inhibitors have previously been evaluated for tumour imaging and therapy. However, the latter application has so far necessitated the use of local or intratumoural delivery, or required multiple administrations of large activities. This maybe improved upon. With this in mind, we present the synthesis, radiosynthesis and preclinical evaluation of iodine-123 labelled rucaparib analogue, 8-[^{123}I]iodo-5-(4-((methylamino)methyl) phenyl)-2,3,4,6-tetrahydro-1H-azepino[5,4,3-*cd*]indol-1-one, [^{123}I] **GD1**, as a potential radiotracer for RLT, *via* copper mediated radioiodination building on our previous work with [^{18}F]rucaparib [23,24].

2. Material and methods

Unless otherwise indicated, all reagents were purchased from Sigma-Aldrich and used without further purification. Olaparib, rucaparib, veliparib, and talazoparib were purchased from Stratech Scientific Ltd. (UK). Sodium [^{123}I]iodide was produced by GE Healthcare as no carrier added [^{123}I]sodium iodide in 0.05 M NaOH. Radiosynthesis was performed using a NanoTek® automated microfluidic device (Advion). HPLC analysis was performed using a Dionex Ultimate 3000 dual channel HPLC system equipped with shared autosampler, parallel UV-detectors and LabLogic NaI/PMT-radiodetectors with FlowRam analog output. The radio-signal is offset by 0.1–0.3 min from the UV signal. All reported activity yields (AYs) and radiochemical yields (RCYs) are non-decay corrected.

2.1. Synthesis of GD1

GD1 was prepared as described in SI.

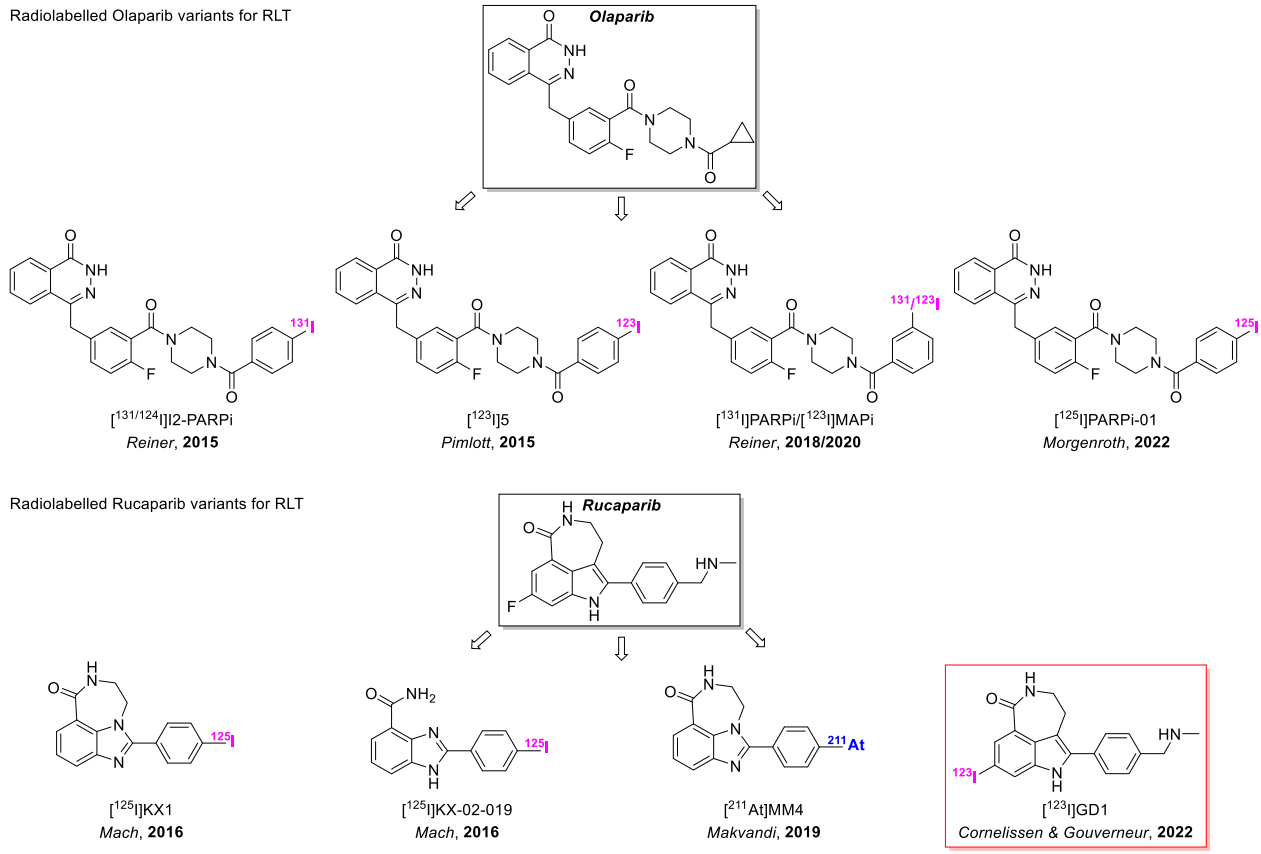

Fig. 1. Olaparib- and Rucaparib-based PARP-targeted RLT agents. In 2022 Hoffman and co-workers have described a bromine-77 labelled rucaparib-derived PARP inhibitor, but chemical structure has not been disclosed yet [29].

2.2. Radiosynthesis of [^{123}I]GD1

[^{123}I]**GD1** was synthesized as described in Fig. 2. A stock solution of $Cu(OCOCF_3)_2$ (14 mg, 0.05 mmol) and 1,10-phenanthroline (8 mg, 0.044 mmol) in MeOH:H_2O (4:1, 10 mL) was freshly prepared. Of this stock solution, 0.3 mL was used to rinse and collect [^{123}I]NaI into a V-vial containing a magnetic stirrer bar and tert-butyl methyl(4-(1-oxo-8-(4,4,5,5-tetramethyl-1,3,2-dioxaborolan-2-yl)-2,3,4,6-tetrahydro-1H-azepino[5,4,3-*cd*]indol-5-yl)benzyl)carbamate precursor **10** (4 mg, 7.5 μmol, see SI), the synthesis of which has been described by us before [23]. The reaction vial was heated to 80 °C with stirring for 30 min. Trifluoro acetic acid (300 mL) was added and the reaction mixture was stirred at 80 °C for a further 25 min. The reaction mixture was dried under nitrogen flow at 105 °C for 5 min, diluted with 0.5 mL of MeCN/H_2O (45:55) and purified by HPLC employing a Gemini LC 250 × 10-mm column (Phenomenex) with flow rate 4 mL/min, monitoring with UV (220 nm) and radioactive traces. [^{123}I]**GD1** was obtained with an activity yield of 45 % and a molar activity up to 20 GBq/mmol over two steps in 150 min. HCl (1 M, 100 mL) was added during ethanol evaporation, just before the final reformulation step with 10 % DMSO in phosphate buffer saline (PBS).

2.3. Cell-free inhibition assay

A commercially available PARP-1 Chemiluminescent Assay Kit (BPS Bioscience, catalog #80551, San Diego, CA, USA) was employed to measure catalytic inhibition of PARP activity by **GD1** compared to rucaparib, following the manufacturer's instructions.

2.4. Cell culture

Human pancreatic ductal adenocarcinoma cells AsPC-1 and PSN-1, and non-small cell lung carcinoma H1299 cells were purchased from ATCC (UK) and maintained in Roswell Park Memorial Institute (RPMI) cell culture medium supplemented with 10 % fetal bovine serum (FBS, Gibco), 2 mM L-glutamine, 100 units/mL penicillin, and 0.1 mg/mL streptomycin (Gibco). Oesophageal adenocarcinoma cells FLO-1 and OE-33 were kindly provided by Professor Katherine Vallis (University of Oxford). H1299, and FLO-1 cells were maintained in Dulbecco's Modified Eagle Medium (DMEM) with 10 % fetal bovine serum (FBS, Gibco), 2 mM L-glutamine, 100 units/mL penicillin, and 0.1 mg/mL streptomycin (Gibco). OE-33 cells were maintained in RPMI supplemented with 10 % FBS (Gibco), 2 mM L-glutamine, 100 units/mL penicillin, and 0.1 mg/mL streptomycin (Gibco). Cells were grown in a humidified environment at 37 °C and 5 % CO_2. Cells were harvested and passaged using trypsin-EDTA solution and were used no >25 passages following resuscitation from liquid nitrogen storage. Cells were authenticated by the provider and additional STR profiling and tested regularly for the absence of mycoplasma contamination.

2.5. Western blot

Western blot analysis was performed to compare the total PARP-1 and PARP-2 expression between cell lines. Total protein lysates were prepared at 4 °C using RIPA buffer (50 mM Tris – pH 8.0, 1 % NP40, 0.5 % sodium deoxycholate, 0.1 % sodium dodecyl sulphate, 150 mM sodium chloride, and complete protease inhibitor cocktail (Sigma-Aldrich)) and extracts were clarified by centrifugation (8000 rpm at 4 °C for 5 min). Protein concentrations were measured using the BCA protein assay (Thermo Scientific) and normalised with RIPA buffer. Protein lysates were denatured in NuPage® LDS sample buffer (Invitrogen) with heating at 100 °C for 5 min, then 30 μg samples were resolved on a NuPage® 4–12 % Bis-Tris gel in MOPS running buffer (Novex) and transferred to PVDF membrane at 20 V for 10 min using an iBlot2 system (Invitrogen). Membranes were blocked in 5 % skimmed milk in PBS with 5 % Tween-20 (PBST) then western blot was performed using the following antibodies: anti-PARP-1 antibody (HPA045168; 1:500); anti-PARP-2 antibody (HPA052003; 1:500) (Atlas Antibodies-Sigma Aldrich, UK), and secondary goat anti-rabbit-HRP antibody (1:3000 dilution; R&D Systems HAF008). All blots were repeated on at least two separate occasions with new cell lysates for validation. To control sample loading and protein transfer, the membranes were also stained for b-Actin (1:1000, clone 3E5, 5125S, Cell Signalling Technologies).

2.6. In vitro uptake and binding selectivity of [^{123}I]GD1

AsPC-1 and PSN-1 cells were added separately to 24-well plates (5 × 10^4 cells/well) with 300 μL growth medium and allowed to adhere overnight. Cells were washed twice and exposed to [^{123}I]**GD1** (33 nM, 25.1 GBq/μmol in a total of 300 μL growth medium) and incubated at 37 °C for increasing lengths of time (0 to 120 min). To assess [^{123}I]**GD1** binding selectivity, unlabelled PARP inhibitors were added in excess (100 μM) for 60 min at 37 °C before addition of [^{123}I]**GD1** (33 nM, 25.1 GBq/μmol in growth medium), and the cells incubated at 37 °C for 60 min. Cell culture medium was removed and cells were washed with PBS twice. Cells were lysed using RIPA buffer (300 mL) for 15 min at room temperature, then washed with PBS (300 μL) and the amount of ^{123}I in the cell lysates was measured using an Wizard2 Automatic Gamma Counter (PerkinElmer). Uptake in AsPC-1, PSN-1, H1299, FLO-1 and OE-33 cells was additionally measured following exposure to [^{123}I]**GD1** (75 nM, 13.1 GBq/μmol in a total of 300 μL growth medium) following the above procedure.

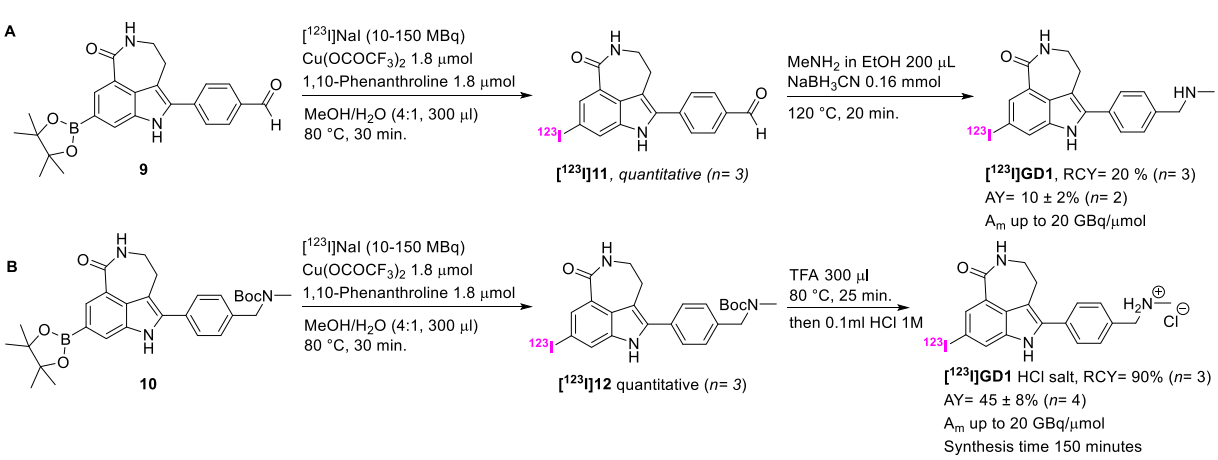

Fig. 2. A) Radiosynthesis of [^{123}I]**GD1** from precursor **9**, B) Radiosynthesis of [^{123}I]**GD1** from precursor **10**.

2.7. Cell retention of [^{123}I]GD1

AsPC-1 and PSN-1 cells were seeded as above and exposed to [^{123}I]**GD1** (33 nM, total 300 μL, 25.1 GBq/μmol) for 60 min. Cell culture medium was removed, and cells were washed with PBS, followed by the addition of fresh growth medium (300 μL). Cells were then further incubated at 37 °C. Cell culture medium was removed and cells were washed with PBS at different times (0–24 h). Cells were lysed and the amount of ^{123}I in the lysates was measured as above. Using these results, radiation absorbed doses were calculated for PSN-1 and AsPC-1 cells, over the 24 h range. S values were obtained from the report by Goddu et al. [30], assuming a cell radius (R_C) of 8 mm and a cell nucleus radius (R_N) of 6 mm.

2.8. Clonogenic survival following exposure to [^{123}I]GD1

AsPC-1, PSN-1, H1299, FLO-1 and OE-33 cells were exposed separately, in aliquots of 5×10^3 cells in a 0.5 mL Eppendorf, to [^{123}I]**GD1** (13.1 GBq/μmol) at different concentrations (0.025–1.2 MBq) in a total volume of 300 mL of growth medium. Cells were incubated with [^{123}I]**GD1** at 37 °C for 60 min. After one hour the tube was centrifugated (5000 rpm, 5 min), medium was removed, followed by the addition of fresh growth medium and cells were then seeded in 6-well plates, in a total of 2 mL growth medium. Cells were incubated at 37 °C for 10 days, washed once with 300 mL PBS, twice with 300 mL ddH_2O, and stained with 1 mL of crystal violet solution overnight, and washed three times with water. The number of colonies relative to control conditions and relative to the number of cells seeded was determined using a Gelcount system.

2.9. SPECT/CT imaging and biodistribution of [^{123}I]GD1

All animal procedures were performed in accordance with the U.K. Animals (Scientific Procedures) Act 1986 and with local ethical committee approval. C57BL/6 mice ($n = 3$, all male) aged 15–20 weeks were purchased from a UK supplier. Animals were housed in IVC cages, up to 6 per cage, in an artificial day-night cycle facility. Food and water were provided *ad libitum*. Mice were administered [^{123}I]**GD1** (1.16–1.42 MBq in 100 μL of PBS, $A_m = 7$ GBq/μmol, DMSO concentration < 10 %) by intravenous injection *via* the lateral tail vein (n = 3). Dynamic SPECT images (over 2 h) were acquired using a MILabs VECTor4 camera, equipped with an ultra-high resolution rat/mouse collimator (1.8 mm), followed by a cone-beam CT scan (55 kV, 0.19 mA) for anatomical reference and attenuation correction. Anaesthesia was maintained using 2.5 % isoflurane throughout the duration of image acquisition. SPECT images were reconstructed using U-SPECT-Rec3.22 software (MILabs, Utrecht, The Netherlands), applying a pixel-based algorithm, ordered subset expectation maximization (OSEM) with 4 subsets, 4 iterations and 0.6 mm voxel size for Iodine-123 (energy window settings 141.3–172.7 keV). Reconstructed SPECT and CT images were viewed and analysed using PMOD v.3.37 (PMOD Technologies, Zurich, Switzerland). Either 2 h or 24 h after radiolabelled compound injection (1.16–3.63 MBq in 100 μL of PBS, $A_m = 7$–9 GBq/μmol), animals were euthanised. Selected organs, tissues and blood were removed, and the percentage of the injected dose per gram of tissue (%ID/g) was determined, using a HIDEX automated gamma counter from Perkin Elmer.

3. Statistical analysis

All data was obtained at least in triplicate. All statistical analyses and nonlinear regression were performed using GraphPad Prism v9 (GraphPad Software, San Diego, CA, USA). Data were tested for normality and analysed as appropriate by one-way ANOVA analysis. Results are reported as mean ± SD, unless stated otherwise.

4. Results

4.1. Radiosynthesis

Radiosynthesis modified from that developed previously for [^{18}F]rucaparib [23] resulted in [^{123}I]**GD1**. Two radiosynthetic approaches were tested: a two-step radiolabelling from the appropriate boronic pinacol ester containing an aldehyde handle to be further functionalized (precursor **9**), and another from a Boc-protected benzylamine boronic pinacol ester (precursor **10**) followed by deprotection (Fig. 2). With both precursors **9** and **10** in hand, we set up a series of pilot experiments using each precursor under different copper-mediated radioiodination conditions previously described by Wilson. et al. [31] Radioiodination of precursor **9** quantitively yielded the radioactive aldehyde intermediate [^{123}I]**11** (Fig. 2A), yet when this underwent reductive amination, no conversion to the product was observed. Instead, degradation of [^{123}I]**11** and a high amount of inorganic iodine-123 were detected by radio-HPLC. We reasoned that the presence of the copper may interfere with the second step, therefore, a passage through a filter (0.22 mM porous diameter) helped the process by removing all precipitate formed during the first reaction step. [^{123}I]**11** then reacted in the reductive amination step, obtaining for the first time [^{123}I]**GD1** in a 20 % radiochemical yield (RCY) by HPLC with an activity yield (AY) after semi-preparative HPLC of 10 % and a molar activity (A_m) of 20 GBq/mmol. Precursor **10** behaved similarly under radioiodination conditions quantitatively yielding [^{123}I]**12** (Fig. 2B). [^{123}I]**GD1** was obtained by deprotection with TFA, with a 90 % radiochemical yield (based on HPLC analysis of the crude product) and only small traces of free iodine were observed. When precursor **10** was evaluated in radiosynthesis followed by preparative HPLC purification, [^{123}I]**GD1** was synthesized in 150 ± 10 min (n = 4) isolated with radiochemical purity always higher than 95 % and it was afforded in 45 % ± 7 % (n.d.c., n = 4) AY and A_m ranging from 7 to 84 GB/μmol. At the end of the radiosynthesis we observed some precipitate. Rucaparib possesses a low water solubility and the introduction of an iodine atom seemed to have decreased this even more, causing precipitation [32]. Since rucaparib is usually administrated in clinic as camsylate salt, this problem was investigated by changing the final reformulation of [^{123}I]**GD1**. Rucaparib solubility is enhanced by salt formation and HCl salt is capable of increasing solubility up to 4 times, as shown in patent [33]. With this in mind, 100 mL of 1.0 M HCl aq. was added during ethanol evaporation, just before the final reformulation step with 10 % DMSO in PBS. The soluble [^{123}I]**GD1** HCl salt's purity and identity was confirmed by radio-HPLC before and after acid addition.

4.2. In vitro evaluation of [^{123}I]GD1

A first *in vitro* uptake assay of [^{123}I]**GD1** on PSN-1 and AsPC-1 cell lines shown a plateau reached within one hour. The higher amount of radiolabelled compound was absorbed by PSN-1, around 20 pmol/cell. (Fig. 3A). A second set of experiments was performed to understand if increased uptake is observed when higher amounts of [^{123}I]**GD1** are presented to the cells. A comparison between two different concentrations (33 nM, 25.1 GBq/μmol *vs* 75 nM 13.1 GBq/mmol) is shown in Fig. 3B underlying a massive variance in radioactive compound uptake when [^{123}I]**GD1** is more concentrated (20 pmol/cell *vs* 228 pmol/cell for PSN-1). When this higher concentration was presented to other cancerous cell lines, H1299, FLO-1 and OE-33, [^{123}I]**GD1** uptake was >50 pmol/cell (Fig. 3C). [^{123}I]**GD1** efflux was fast at first for all cell lines, in the first hour the concentration dropped almost by half (to 6–9 pmol/cell). The activity in the cells then decreased slowly to 5 pmol/cell over 2 h, consistent with first-order efflux. At 24 h, a small amount of compound, around 0.5–1 pmol/cell, was still present (Fig. 3D).

The ability of non-radiolabelled **GD1** to inhibit the catalytic activity of PARP-1 in a cell-free system was initially compared with rucaparib as a proxy for their binding affinity. This showed IC_{50} values of 239 nM and

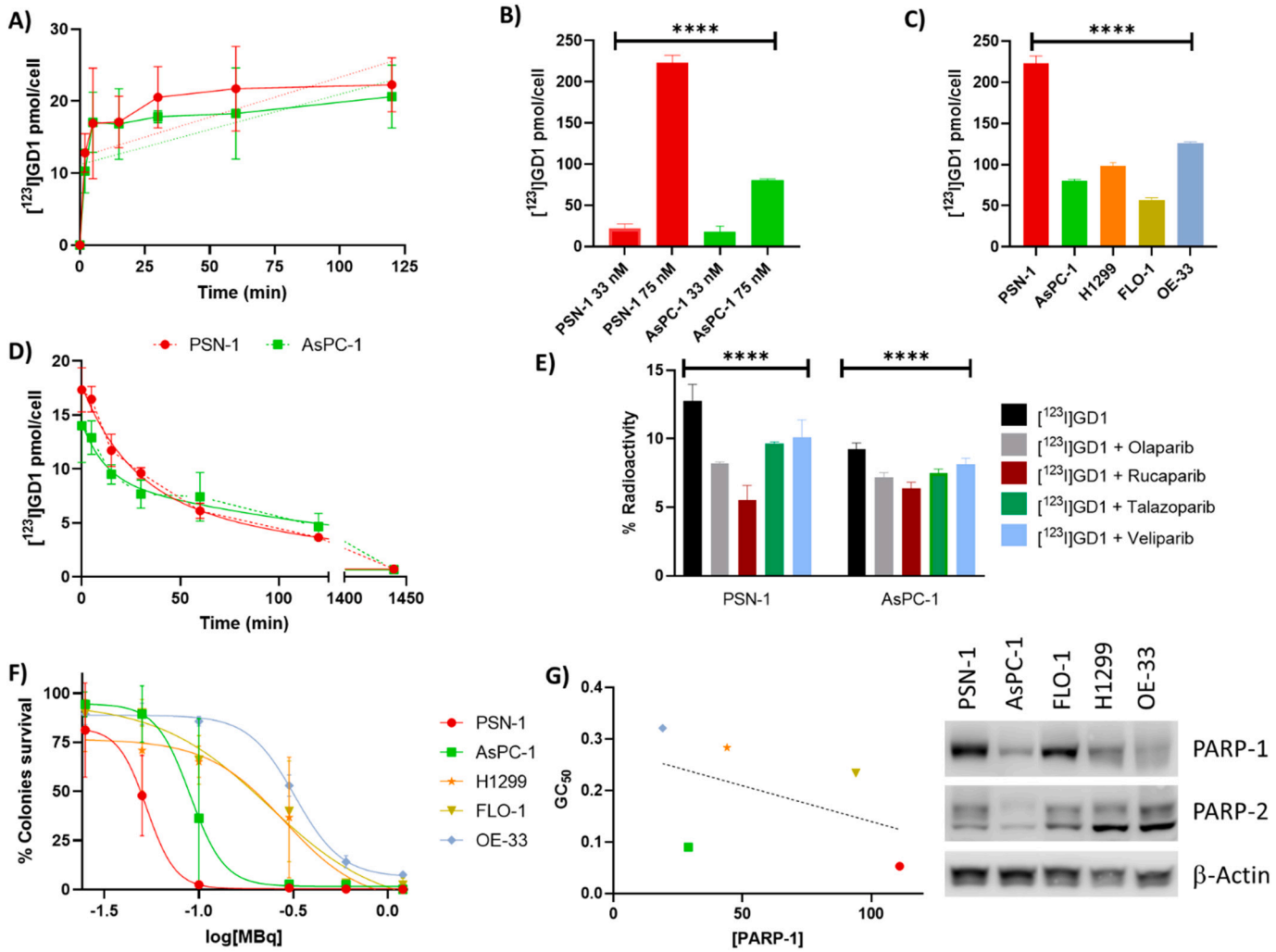

Fig. 3. A) Uptake of [^{123}I]**GD1** (33 nM, 25.1 GBq/μmol) in PSN-1 and AsPC-1 cells over 2 h. B) Uptake of [^{123}I]**GD1** 33 nM, 25.1 GBq/μmol *vs* 75 nM 13.1 GBq/mmol in PSN-1 and AsPC-1 cell lines. C) Uptake assay of [^{123}I]**GD1** (75 nM 13.1 GBq/mmol) in PSN-1, ASPC-1, H1299, FLO-1 and OE-33 cell lines. D) Retention of [^{123}I]**GD1** (33 nM, 25.1 GBq/μmol) in selected cell lines over 24 h. E) Blocking of [^{123}I]**GD1** (33 nM, 25.1 GBq/μmol) uptake in PSN-1 and AsPC-1 cells with one of a panel of cold, unlabelled PARP inhibitors (100 μM). F) Representative clonogenic survival following a one-hour exposure to [^{123}I]**GD1** (75 nM 13.1 GBq/mmol). G) PARP-1 expression in different cell lines *vs* calculated GC_{50} from clonogenic survival assay and western blot of PARP-1 and PARP-2 protein expression in PSN-1, ASPC-1, H1299, FLO-1 and OE-33 cell lines. Asterisks indicate levels of significance: *, $P < 0.05$; **, $P < 0.01$; ***, $P < 0.001$; and ****, $P < 0.0001$.

1.07 nM, for **GD1** and rucaparib, respectively [34], for PARP-1 inhibition (see SI).

Binding selectivity of [^{123}I]**GD1** was also evaluated by blocking assay with structurally different PARP inhibitors, olaparib, rucaparib, talazoparib and veliparib (Fig. 3E). Partial blocking of [^{123}I]**GD1** uptake was shown by a panel of PARP inhibitors, however they were unable to significantly reduce the radioactive signal in all the cell lines [22,31]. Radiation absorbed doses *in vitro* were calculated as 1.54–23.1 Gy for PSN-1 and from 1.25 Gy - 18.7 Gy for AsPC-1 cells.

4.3. Clonogenic survival

[^{123}I]**GD1** significantly reduced colony formation of PSN-1 and AsPC-1, with a GC_{50} of 52 kBq (95 % CI 22–66) for PSN-1 and GC_{50} of 89 kBq (95 % CI 18–130) for AsPC-1 (Fig. 3F). H1299, FLO-1 and OE-33 cell lines were less susceptible to [^{123}I]**GD1** with a GC_{50} up to 312 MBq (95% CI 297–354) for OE-33 cells (Fig. 3F).

4.4. Western blot analysis

Western blot revealed that expression of PARP-1 was higher in PSN-1 and FLO-1 cells than others, consistent with previously reported data [24], while expression of PARP-2 was higher in OE-33 and H1299 (Fig. 3G). PARP-1 expression was plotted *versus* GC_{50} obtained from experimental results, apart from AsPC-1 and FLO-1, the other cell lines OE-33, H1299 and PSN-1 potentially fit more in the correlation between a low GC_{50} and high PARP-1 expression (Fig. 3G).

4.5. In vivo evaluation

[^{123}I]**GD1** biodistribution was characterized *in vivo* in C57BL/6 mice at 2 and 24 h following an intravenous bolus administration. SPECT-CT imaging showed renal and hepatobiliary clearance (Fig. 4A and B), with biphasic blood clearance with a calculated weighted half-life of 1.7 min (95 % CI, 1.2–2.8 min) (Fig. 4C). The same biphasic pattern was found also in [^{18}F]Rucaparib with a slightly longer calculated weighted half-life of 4.3 min [23].

5. Discussion

We found precursor **10** to be a superior starting material for the radiosynthesis of [^{123}I]**GD1**, through copper-mediated radioiodination.

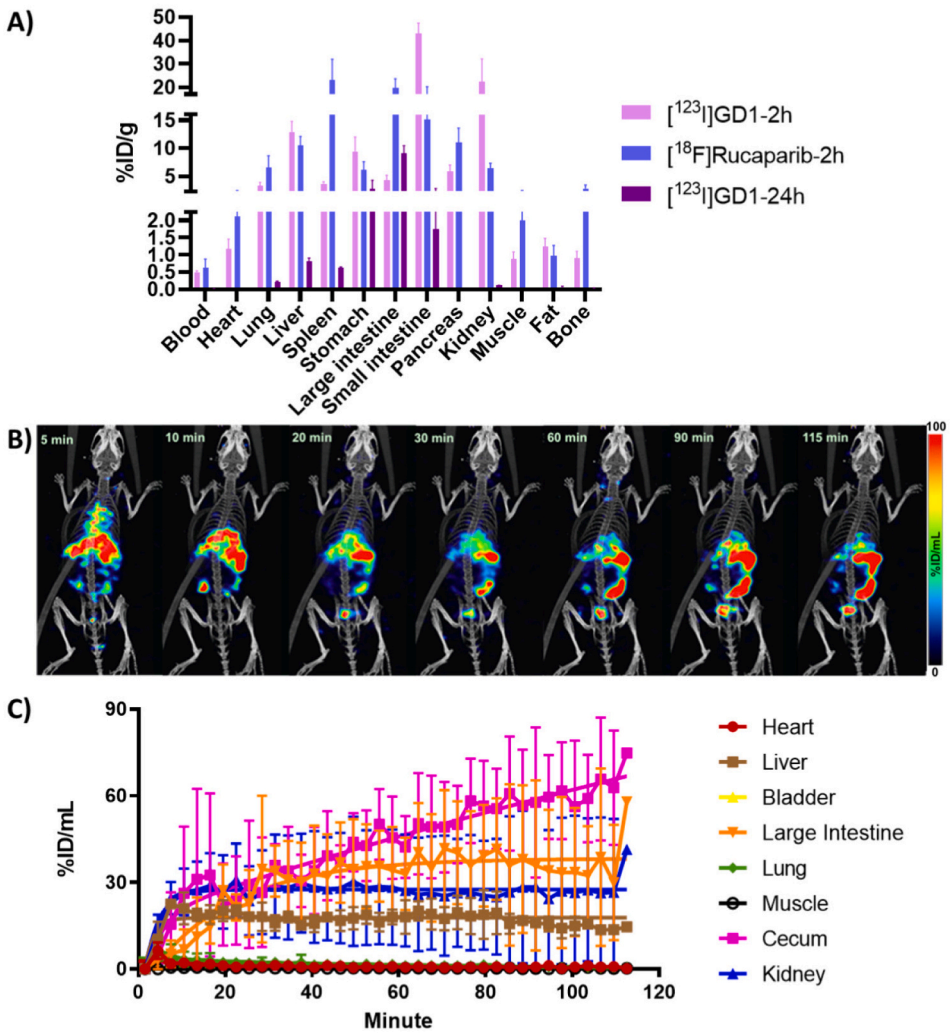

Fig. 4. *In vivo* studies evaluating [^{123}I]**GD1** biodistribution in wild type mice. A) Biodistribution of [^{123}I]**GD1** in selected tissues in wildtype mice, 2 or 24 h after intravenous administration of [^{123}I]**GD1** (1.3 MBq, 7 GBq/μmol), compared to [^{18}F]rucaparib [24]. B) SPECT/CT scan images, following intravenous administration of 1.16–3.63 MBq in 100 μL of PBS, A_m = 7–9 GBq/μmol. C) Time activity curves based on VOI analysis of dynamic SPECT images (n = 3).

Precursor **9** was susceptible to the presence of metal traces as possible promoters of side-reactions [21,25]. Copper itself has a limited ability to participate in haloarene functionalization, and this behaviour has been attributed to its relatively low rate of oxidative addition in comparison to other metals such as nickel and palladium [35,36]. Indeed, the most robust copper cross-coupling reactions are limited to transmetallating reagents such as organoboronic acids or esters, specifically to bypass the challenge of oxidative addition [37]. Even if elegant studies have allowed for improvements in the rate of oxidative addition for certain substrate classes, functionalization of aryl halides by copper catalysis remains largely restricted to aryl iodides and activated aryl bromides under harsh reaction conditions [38]. We reasoned that the presence of copper may interfere with the reductive amination step leading to a coupling side reaction between [^{123}I]**11** and the starting material **9**, which can also explain the loss of iodine-123 from the molecule. The presence of Boc-protected benzylamine chain in precursor **10** circumvents these problems, leading to robust radiosynthesis of [^{123I}]**GD1**.

Consistent with previously reported data [24], an increased concentration of radiotracer given to cancer cells resulted in increased cell uptake of radioactive material as shown in Fig. 3B. We may explain the different [^{123}I]**GD1** uptake ratio between PSN-1 and AsPC-1 by the non-identical PARP-1 expression, where we had a similar trend for both [^{18}F]rucaparib uptake in the same cell lines and [^{18}F]Olaparib uptake in U251MG compared to U87MG cells [39]. However, when [^{123}I]**GD1** was tested on other cell lines such as H1299, FLO-1 and OE-33 the degree of uptake observed was intriguing since the correlation cited before was more blurred. We hypothesise that this may be due to differences in intrinsic expression of PARP-1 and 2 in the selected cell lines, off-target binding of [^{123}I]**GD1**, PARP trapping effects and potential upregulation of PARP expression for DNA damage response caused by radiation [38]. The retention assay showed a good ability of [^{123}I]**GD1** to remain in cells, potentially trapped to DNA. Only cell-level dosimetry analysis were performed using experimental data from retention assay. The calculated absorbed doses for both PSN-1 and AsPC-1 cell lines are in line with the ones obtained experimentally from Pirovano and co-workers [15] using [^{123}I]MAPi for glioblastoma treatment supporting the high-LET of iodine-123 as Auger emitter which may also reflect a high relative biological effectiveness [40,41].

The modest ability of **GD1** to interact with PARP-1 is likely explained by the switch of a fluorine atom with an iodine. This replacement not only brings a change in the electronic properties but also in the atom size (F = 147 pm *vs.* *I* = 198 pm), presumably hampering the interactions with **GD1** in the PARP-1 catalytic pocket since the fluorine atom of rucaparib fills a small cavity present in the binding site (defined by

Phe897, Ala898, Lys903, and Glu988 residues in PARP-1) [42]. As expected, *in vitro* blocking of [^{123I}]**GD1** resulted in only partial blocking of the radioactive molecule by an excess of a variety of PARP inhibitors, in agreement with the inhibition binding assay, confirming possible non-specific or off-target specific binding.

Clonogenic survival of pancreatic cancer cells after exposure to [^{123}I]**GD1** showed promising results. [^{123}I]**GD1** significantly reduced colony formation in both PSN-1 and AsPC-1 cells, with GC_{50} values in the kBq range. Previously, several pre-clinical studies demonstrated the use of radiolabelled modified PARP inhibitors to reduce tumour growth in high-PARP expressions malignancies [12–18]: for example, [^{123}I]MAPi was used on glioblastoma cancer cells U251 and it possess a comparable clonogenic survival reduction with [^{123}I]**GD1**, a GC_{50} slightly higher than 50 kBq [15]. On the other hand, the group of Makvandi showed that [^{125}I]KX1can inhibit cell colonies formation with a GC_{50} around 13 kBq, while the iodine-123 labelled counterpart was not reported [43]. As expected selective PARP inhibitors bearing potent a particle, such as astatine-211, display a high cytotoxicity using just a few kilobecquerels of radioactive agent [19]. Recently, Hoffman and co-workers have reported a bromine-77 labelled version of PARPi, this compound was screened on several cell lines showing a general GC_{50} higher than 100 kBq [29]. Although FLO-1 cells showed lower PARP-1 expression levels compared to PSN-1 by western blot, the former were less susceptible towards [^{123}I]**GD1**, the possible explanations for such disparity may be the result of higher PARP-2 levels, or other genomic differences and intrinsic radiosensitivity. The reasons for such discrepancies warrant additional investigation [16].

Biodistribution (Fig. 4A) together with dynamic imaging (Fig. 4B) following administration of [^{123}I]**GD1** to wild type C57BL/6 mice (n = 3) showed that [^{123}I]**GD1** is eliminated *via* hepatobiliary and renal pathways. The clearance pattern of [^{123}I]**GD1** over 2 h is similar to that of [^{18}F]rucaparib [23], but signal from [^{123}I]**GD1** was lower at 2 h post administration in the spleen, large intestine, pancreas and muscle, while it was more present in small intestine and kidneys, when compared with its radiofluorinated counterpart. At 24 h, [^{123}I]**GD1** resides mainly in the abdominal region, explained by its more lipophilic character [36]. The prolonged retention of [^{123}I]**GD1** in the body, mainly concentrated in the abdominal region, could possibly lead to long term toxicity due to radiation. However, due to its shorter half-life and absence of beta particles, ^{123}I carries a reduced radiation burden to normal tissue compared to beta or alpha-emitting radionuclides, allowing for a higher administered activity [44].The development of PARP inhibitors bearing AE emitters as theragnostic shows great potential for the fight against cancer [45,46,47].

6. Conclusion

Here, we evaluated a new theragnostic agent based on a rucaparib-like scaffold and in preclinical models of cancer. Taken together, *in vitro* and *in vivo* studies demonstrated the potential of [^{123}I]**GD1** as a possible theragnostic agent, showing a pharmacodynamics and *in vitro* uptake similar to [^{18}F]rucaparib. [^{123}I]**GD1** may have potential as a theragnostic agent towards pancreatic cancer cell lines, warranting further investigation.

Funding

This research was supported by Cancer Research UK through the Oxford Institute for Radiation Oncology, Medical Research Council (MRC) (MR/R01695X/1, G.D. and F.G., and H3R00580, C.Y·C) and Pancreatic Cancer UK (PCUK H3R00510, C.Y·C).

Declaration of competing interest

The authors declare that GD, ZC, CC, FG, VG, and BC own patents on radiolabelled compounds.

Acknowledgements

We acknowledge financial support from Cancer Research UK through the Oxford Institute for Radiation Oncology, Medical Research Council (MRC) (MR/R01695X/1, G.D. and F.G.) and Pancreatic Cancer UK (PCUK H3R00510, C.Y·C).

References

[1] Kosj Y, Showalter TN, Ohri N. Radiation therapy intensification for solid tumors: a systematic review of randomized trials. Int J Radiat Oncol Biol Phys 2015;93:737–45. https://doi.org/10.1016/j.ijrobp.2015.07.2284.
[2] Anand S, Chan TA, Hasan T, Maytin E, v.. Current prospects for treatment of solid tumors via photodynamic, photothermal, or ionizing radiation therapies combined with immune checkpoint inhibition (A review). Pharmaceuticals 2021;14:447. https://doi.org/10.3390/ph14050447.
[3] Elbanna M, Chowdhury NN, Rhome R, Fishel ML. Clinical and preclinical outcomes of combining targeted therapy with radiotherapy, front. Oncologia 2021:11. https://doi.org/10.3389/fonc.2021.749496.
[4] Mohan G, Narayanasamy A, Vellingiri B. Recent advances in radiotherapy and its associated side effects in cancer—a review. J Basic Appl Zool 2019;80:14. https://doi.org/10.1186/s41936-019-0083-5.
[5] Gudkov SV, Shilyagina NY, Vodeneev VA, Zvyagin AV. Targeted radionuclide therapy of human tumors. Int J Mol Sci. 2016;17:33. https://doi.org/10.3390/ijms17010033.
[6] Ersahin D, Doddamane I, Cheng D. Targeted radionuclide therapy. Cancers (Basel) 2011;3:3838–55. https://doi.org/10.3390/cancers3043838.
[7] Cornelissen B, Vallis KA. Targeting the nucleus: an overview of auger-electron radionuclide therapy. Curr Drug Discov Technol 2010;7:263–79. https://doi.org/10.2174/157016310793360657 2010.
[8] Kassis AI. The amazing world of auger electrons. Int J Radiat Biol 2004;80:789–803. https://doi.org/10.1080/09553000400017663.
[9] Rigby A, Blower JE, Blower PJ, Terry SYA, Abbate V. Targeted auger electron-emitter therapy: radiochemical approaches for thallium-201 radiopharmaceuticals. Nucl Med Biol 2021;98:1–7. https://doi.org/10.1016/j.nucmedbio.2021.03.012.
[10] Jannetti SA, Zeglis BM, Zalutsky MR, Reiner T. Poly(ADP-ribose)polymerase (PARP) inhibitors and radiation therapy. Front Pharmacol 2020;11:170. https://doi.org/10.3389/fphar.2020.00170.
[11] Lord CJ, Ashworth A. PARP inhibitors: synthetic lethality in the clinic. Science 2017;355:1152–8. https://doi.org/10.1126/science.aam7344.
[12] Underhill C, Toulmonde M, Bonnefoi H. A review of PARP inhibitors: from bench to bedside. Ann Oncol 2011;22:268–79. https://doi.org/10.1093/annonc/mdq322.
[13] Cornelissen B, Kersemans V, Darbar S, Smart S, Vallis KA. Molecular radiation therapy: targeting DNA damage response proteins. Cancer Res 2010;70:5771. https://doi.org/10.1158/1538-7445.AM10-5771.
[14] Salinas B, Irwin CP, Kossatz S, Bolaender A, Chiosis G, Pillarsetty N, Weber WA, Reiner T. Radioiodinated PARP1 tracers for glioblastoma imaging. EJNMMI Res 2015;46:5. https://doi.org/10.1186/s13550-015-0123-1.
[15] Pirovano G, Jannetti SA, Carter LM, Sadique A, Kossatz S, Guru N, de Souza França PD, Maeda M, Zeglis BM, Lewis JS, Humm JL, Reiner T. Targeted brain tumor radiotherapy using an auger emitter. Clin Cancer Res 2020;26:2871–81. https://doi.org/10.1158/1078-0432.CCR-19-2440.
[16] Jannetti SA, Carlucci G, Carney B, Kossatz S, Shenker L, Carter LM, Salinas B, Brand C, Sadique A, Donabedian PL, Cunanan KM, Gönen M, Ponomarev V, Zeglis BM, Souweidane MM, Lewis JS, Weber WA, Humm JL, Reiner T. PARP-1-targeted radiotherapy in mouse models of glioblastoma. J Nucl Med 2018;59:1225–33. https://doi.org/10.2967/jnumed.117.205054.
[17] Lee H, Riad A, Martorano P, Mansfield A, Samanta M, Batra V, Mach RH, Maris JM, Pryma DA, Makvandi M. PARP-1-targeted auger emitters display high-LET cytotoxic properties in vitro but show limited therapeutic utility in solid tumor models of human neuroblastoma. J Nucl Med 2020;61:850–6. https://doi.org/10.2967/jnumed.119.233965.
[18] Makvandi M, Xu K, Lieberman BP, Anderson RC, Effron SS, Winters HD, Zeng C, McDonald ES, Pryma DA, Greenberg RA, Mach RH. A radiotracer strategy to quantify PARP-1 expression in vivo provides a biomarker that can enable patient selection for PARP inhibitor therapy. Cancer Res 2016;76:4516–24. https://doi.org/10.1158/0008-5472.CAN-16-0416.
[19] Makvandi M, Lee H, Puentes LN, Reilly SW, Rathi KS, Weng CC, Chan HS, Hou C, Raman P, Martinez D, Xu K, Carlin SD, Greenberg RA, Pawel BR, Mach RH, Maris JM, Pryma DA. Targeting PARP-1 with alpha-particles is potently cytotoxic to human neuroblastoma in preclinical models. Mol Cancer Ther 2019;18:1195–204. https://doi.org/10.1158/1535-7163.MCT-18-0837.
[20] Sankaranarayanan RA, Peil J, Vogg ATJ, Bolm C, Terhorst S, Classen A, Bauwens M, Maurer J, Mottaghy F, Morgenroth A. Auger emitter conjugated PARP inhibitor for therapy in triple negative breast cancers: a comparative in-vitro study. Cancers (Basel). 2022;4:230. https://doi.org/10.3390/cancers14010230.
[21] Wilson TC, Xavier MA, Knight J, Verhoog S, Torres JB, Mosley M, Hopkins SL, Wallington S, Allen PD, Kersemans V, Hueting R, Smart S, Gouverneur V, Cornelissen B. PET imaging of PARP expression using 18F-olaparib. J Nucl Med 2019;60:504–10. https://doi.org/10.2967/jnumed.118.213223.
[22] Guibbal F, Hopkins SL, Pacelli A, Isenegger PG, Mosley M, Torres JB, Dias GM, Mahaut D, Hueting R, Gouverneur V, Cornelissen B. [18F]AZD2461, an insight on

difference in PARP binding profiles for DNA damage response PET imaging. Mol Imaging Biol 2020;20:1226–34. https://doi.org/10.1007/s11307-020-01497-6.
[23] Chen Z, Destro G, Guibbal F, Chan CY, Cornelissen B, Gouverneur V. Copper-mediated radiosynthesis of [18F]Rucaparib. Org Lett 2021;23:7290–4. https://doi.org/10.1021/acs.orglett.1c02770.
[24] Chan CY, Chen Z, Destro G, Veal M, Lau D, O'Neill E, Dias G, Mosley M, Kersemans V, Guibbal F, Gouverneur V, Cornelissen B. Imaging PARP with [18F] rucaparib in pancreatic cancer models. Eur J Nucl Med Mol Imaging 2022;49: 3668–78. https://doi.org/10.1007/s00259-022-05835-4.
[25] Ajenjo J, Destro G, Cornelissen B, Gouverneur V. Correction to: Closing the gap between 19F and 18F chemistry (EJNMMI Radiopharmacy and Chemistry, 2021;6: 33, 10.1186/s41181-021-00143-y). EJNMMI Radiopharm Chem 2022;7. https://doi.org/10.1186/s41181-021-00152-x.
[26] Ajenjo J, Destro G, Cornelissen B, Gouverneur V. Closing the gap between 19F and 18F chemistry. EJNMMI Radiopharm Chem 2021;6:33. https://doi.org/10.1186/s41181-021-00143-y.
[27] Chan CY, Tan KV, Cornelissen B. PARP inhibitors in cancer diagnosis and therapy. Clin Cancer Res 2021;27:1585–94. https://doi.org/10.1158/1078-0432.CCR-20-2766.
[28] Nguyen NT, Pacelli A, Nader M, Kossatz S. DNA repair enzyme Poly(ADP-Ribose) polymerase 1/2 (PARP1/2)-targeted nuclear imaging and radiotherapy. Cancers (Basel) 2022;14:1129. https://doi.org/10.3390/cancers14051129.
[29] Hoffman SLV, Mixdorf JC, Makvandi M, Lee H, Aluicio-Sarduy E, Barnhart TE, Patankar MS, Engle JW, Ellison PA. In vitro targeted radionuclide therapy studies of a PARP-targeted Meitner-Auger electron emitting radiopharmaceutical. SNMMI; 2022. poster presentation.
[30] Goddu SM, Howell RW, Rao DV. Cellular dosimetry: absorbed fractions for monoenergetic electron and alpha particle sources and S-values for radionuclides uniformly distributed in different cell compartments. J Nucl Med 1994;35:303–16.
[31] Wilson TC, McSweeney G, Preshlock S, Verhoog S, Tredwell M, Cailly T, Gouverneur V. Radiosynthesis of SPECT tracers: via a copper mediated 123I iodination of (hetero)aryl boron reagents. Chem Commun 2016;52:13277–80. https://doi.org/10.1039/c6cc07417k.
[32] Glyn RJ, Pattison G. The effects on lipophilicity of replacing oxygenated functionality with their fluorinated bioisosteres. J Med Chem 2021;64:10246–59. https://doi.org/10.1021/acs.jmedchem.1c00668.
[33] Griffin RJ, Srinivasan S, Bowman K. Resistance-modifying agents. 5.1 synthesis and biological properties of quinazolinone inhibitors of the DNA repair enzyme poly (ADP-ribose) polymerase (PARP). J Med Chem 1998;41:5247–56. https://doi.org/10.1021/jm980273t.
[34] Valabrega G, Scotto G, Tuninetti V, Pani A, Scaglione F. Differences in parp inhibitors for the treatment of ovarian cancer: mechanisms of action, pharmacology, safety, and efficacy. Int J Mol Sci 2021;22:1. https://doi.org/10.3390/ijms22084203.
[35] Ribas X, Güell I. Cu(I)/Cu(III) catalytic cycle involved in Ullmann-type cross-coupling reactions. In: Pure and Applied Chemistry. 345. IUPAC Secretariat; 2014. p. 360. https://doi.org/10.1515/pac-2013-1104.
[36] Le C, Chen TQ, Liang T, Zhang P, Macmillan DWC. A radical approach to the copper oxidative addition problem: Trifluoromethylation of bromoarenes. Science 2018;360:1010–4. http://science.sciencemag.org/.
[37] Gurung SK, Thapa S, Kafle A, Dickie DA, Giri R. Copper-catalyzed suzuki-miyaura coupling of arylboronate esters: transmetalation with (PN)CuF and identification of intermediates. Org Lett 2014;16:1264–7. https://doi.org/10.1021/ol500310u.
[38] Lavagnino MN, Liang T, Macmillan DWC. HARC as an open-shell strategy to bypass oxidative addition in Ullmann-Goldberg couplings. PNAS 2020;117:21058–64. https://doi.org/10.1073/pnas.2011831117/-/DCSupplemental.
[39] Chan CY, Hopkins SL, Guibbal F, Pacelli A, Baguña Torres J, Mosley M, Lau D, Isenegger P, Chen Z, Wilson TC, Dias G, Hueting R, Gouverneur V, Cornelissen B. Correlation between molar activity, injection mass and uptake of the PARP targeting radiotracer [18F]olaparib in mouse models of glioma. EJNMMI Res 2022; 12:67. https://doi.org/10.1186/s13550-022-00940-9.
[40] Fourie H, Nair S, Miles X, Rossouw D, Beukes P, Newman RT, Zeevaart JR, Vandevoorde C, Slabbert J. Estimating the relative biological effectiveness of auger electron emitter 123I in human lymphocytes. Front Phys. 2020:8. https://doi.org/10.3389/fphy.2020.567732.
[41] Makrigiorgos GM, Kassis AI, Baranowska-Kortylewicz J, Mcelvany KD, Welch MJ, Sastry KSR, Adelstein SJ. Radiotoxicity of 5-[123I]iodo-2'-deoxyuridine in V79 cells: a comparison with 5-[125I]iodo-2'-deoxyuridine. Radiat Res 1989;118: 532–44. https://www.jstor.org/stable/3577411?seq=1&cid=pdf-.
[42] Papeo G, Posteri H, Borghi D, Busel AA, Caprera F, Casale E, Ciomei M, Cirla A, Corti E, D'Anello M, Fasolini M, Forte B, Galvani A, Isacchi A, Khvat A, Krasavin MY, Lupi R, Orsini P, Perego R, Pesenti E, Pezzetta D, Rainoldi S, Riccardi-Sirtori F, Scolaro A, Sola F, Zuccotto F, Felder ER, Donati D, Montagnoli A. Discovery of 2-[1-(4,4-Difluorocyclohexyl)piperidin-4-yl]-6-fluoro-3-oxo-2,3-dihydro-1H-isoindole-4-carboxamide (NMS-P118): a potent, orally available, and highly selective PARP-1 inhibitor for cancer therapy. J Med Chem 2015;58: 6875–98. https://doi.org/10.1021/acs.jmedchem.5b00680.
[43] Riad A, Gitto SB, Lee H, Winters HD, Martorano PM, Hsieh CJ, Xu K, Omran DK, Powell DJ, Mach RH, Makvandi M. PARP theranostic auger emitters are cytotoxic in BRCA mutant ovarian cancer and viable tumors from ovarian cancer patients enable ex-vivo screening of tumor response. Molecules 2020;25. https://doi.org/10.3390/MOLECULES25246029.
[44] Morphis M, van Staden JA, du Raan H, Ljungberg M. Evaluation of Iodine-123 and Iodine-131 SPECT activity quantification: a Monte Carlo study. EJNMMI Phys 2021;8:61. https://doi.org/10.1186/s40658-021-00407-1.
[45] Buchegger F, Perillo-Adamer F, Dupertuis YM, Bischof Delaloye A. Auger radiation targeted into DNA: a therapy perspective. Eur J Nucl Med Mol Imaging 2006;33: 1352–63. https://doi.org/10.1007/s00259-006-0187-2.
[46] Ku A, Facca VJ, Cai Z, Reilly RM. Auger electrons for cancer therapy – a review. EJNMMI Radiopharm Chem 2019;4:27. https://doi.org/10.1186/s41181-019-0075-2.
[47] Salih S, Alkatheeri A, Alomaim W, Elliyanti A. Radiopharmaceutical treatments for cancer therapy, radionuclides characteristics, applications, and challenges. Molecules 2022;27:2660. https://doi.org/10.3390/molecules27165231.